

THE COLD DARK MATTER HALOS OF LOCAL GROUP DWARF SPHEROIDALS

JORGE PEÑARRUBIA¹, ALAN MCCONNACHIE & JULIO F. NAVARRO²

Department of Physics and Astronomy, University of Victoria, 3800 Finnerty Rd., Victoria, BC, V8P 5C2, Canada
Draft version February 7, 2020

ABSTRACT

We examine the dynamics of stellar systems embedded within cold dark matter (CDM) halos in order to assess observational constraints on the dark matter content of Local Group dwarf spheroidals (dSphs). Approximating the stellar and dark components by King and NFW models, respectively, we identify the parameters of dark halos consistent with the kinematics and spatial distribution of stars in dSphs as well as with cosmological N-body simulations. Our analysis shows, in agreement with previous work, that the total mass within the luminous radius is reasonably well constrained and approximately independent of the luminosity of the dwarf, highlighting the poor correspondence between luminosity and halo mass at the extremely faint end of the luminosity function. This result implies that the average density of dark matter is substantially higher in physically small systems such as Draco and Sculptor than in larger systems such as Fornax. Because massive CDM halos are denser than low mass ones at all radii, these results imply that Draco formed in a halo 5 times more massive than Fornax's despite being roughly 70 times fainter. Stellar velocity dispersion profiles ($\sigma_p(R)$) provide further constraints; in systems where data exist, $\sigma_p(R)$ remains flat almost to the nominal "tidal" radius, implying that stars are deeply embedded within their cold dark matter halos and are quite resilient to tidal disruption. We estimate that halos would need to lose more than 90% of their original mass before tides begin affecting the kinematics of stars, but even then the peak circular velocity of the dark halo, V_{\max} , is barely affected. We estimate that V_{\max} is about 3 times higher than the central velocity dispersion of the stars, a result in agreement with previous estimates and that alleviates significantly the CDM "substructure crisis". We use these results to interpret the structural differences between the M31 and Milky Way (MW) dSph population and, in particular, the observation that M31 dwarfs are physically more extended by approximately a factor two than MW dwarfs of similar luminosity. Our modeling indicates that this difference in size should be reflected in their kinematics, and predicts that M31 dwarfs should have velocity dispersions up to a factor of ~ 2 higher than their MW counterparts. This is an eminently falsifiable prediction of CDM-motivated models of dSphs that may be verified with present observational capabilities.

Subject headings:

1. INTRODUCTION

Ever since the first measurements of their velocity dispersion became available (Aaronson 1983, Aaronson & Olszewski 1987), dwarf galaxies in the vicinity of the Milky Way have been a difficult puzzle to piece together in models of galaxy formation. Their relatively large size, low luminosity, and sizable velocity dispersion suggest the presence of large amounts of dark matter (Armandroff, Olszewski & Pryor 1995, see the review of Mateo 1998; for more recent work consult Kleyna et al. 2005, Muñoz et al. 2005, 2006 and references therein). However, the absence of clear correlations between inferred dark matter content and the structural properties of the luminous component have led to arguments about the true physical nature of these objects, and to proposals that many of these faint systems may actually be line-of-sight alignments of unbound stars (e.g., Kroupa 1997 and references therein). Although a consensus now seems to be being reached regarding the true physical nature of these elusive systems, a number of issues regarding the dark matter content of dwarf spheroidals (dSphs, for short), as well as the spatial extent of their dark halos, remain largely unresolved.

These issues were brought into focus when cosmological N-body simulations revealed the presence of substantial substructure in galaxy-sized cold dark matter (CDM) halos (Klypin et al. 1999, Moore et al. 1999). These simulations indicate that *hundreds* of self-bound cold dark matter halos massive enough (in principle) to harbor a dwarf galaxy are expected to populate the halo of the Milky Way, in sharp contrast with the mere *tens* of dwarf galaxies known to orbit the Galaxy. This realization rekindled interest in explaining the detailed correspondence between dark halos and luminous galaxies at the faint end of the luminosity function, an issue that had long been highlighted as a challenge for hierarchical galaxy formation models (White & Rees 1978, Kauffmann, White & Guiderdoni 1993).

The leading scenario for reconciling the discrepancy between "luminous" and "dark" substructure in the Milky Way halo envisions dwarf galaxies as able to form only in halos above a certain mass threshold. The threshold is determined by the need to retain gas and to sustain continuing star formation despite the effects of feedback from evolving stars and the heating from photoionizing radiation (Efstathiou 1992, Bullock, Kravtsov & Weinberg 2000, Somerville 2002, Benson et al. 2002). Adjusting the mass threshold appropriately, the scarcity of luminous dwarfs may be explained by the relatively few mas-

¹ Email: jorpega@uvic.ca

² Fellow of the Canadian Institute for Advanced Research

sive substructure halos that exceed the threshold (Stoehr et al 2002, Hayashi et al 2003, Kazantzidis et al 2004). This is an appealing and elegant solution, and offers a relatively clean prediction that may be tested observationally: most dwarfs at the extreme faint end of the luminosity function should inhabit relatively massive halos, of mass comparable to that defined by the threshold.

For example, given the large spread in luminosity of dwarfs in the Local Group³, and the expectation that they should all inhabit halos of similar mass, this proposal implies that there should be little correlation between the dark matter and luminous content of a dwarf. Massive dark halos would also be more affected by dynamical friction (Peñarrubia, Kroupa & Boily 2002, Zentner & Bullock 2003, Peñarrubia & Benson 2005), leading to a bias in the spatial distribution of dSphs within the halo of the Milky Way relative to the bulk of substructure halos—an effect that may be potentially observable.

Finally, their relatively massive halos would make these extremely faint galaxies more resilient to tidal disruption, suggesting that tidal tails and other obvious evidence of tidal stirring should be present only in systems that have lost most of their original mass by the action of tidal forces. In these models, the “tidal” radii attached by King-model fitting to the surface brightness profiles of dSphs, as well as the “break” radii identified in the outskirts of some dSphs, should reflect just the edge of the luminous component rather than a feature of dynamical significance (e.g. UMi, Martínez-Delgado et al. 2001, Palma et al. 2003; Carina, Majewski et al. 2005). Establishing the dark matter content of dwarf galaxies in the Local Group thus promises to be a fruitful enterprise.

Validating (or refuting) these theoretical expectations through observation is, however, not straightforward. One reason is that few dwarfs have gas on circular orbits and, therefore, stars are the only viable dynamical tracer. The interpretation of the observations is thus complicated by degeneracies between orbital shapes, their radial dependence, and the overall mass profile (Wilkinson et al. 2002, Kazantzidis et al. 2004, Mashchenko et al. 2006, Kleyna et 2004, Tolstoy et al. 2004, Wilkinson et al. 2004, Muñoz et al. 2005, 2006, Wang et al. 2005, Walker et al. 2006a,b, Sohn et al. 2006).

The second reason concerns the fact that these dynamical tracers lie, by definition, within the luminous radius of the dwarfs. Since dark halos are expected to be extended objects reaching far beyond the luminous confines of a galaxy, a certain amount of uncertain extrapolation appears inevitable. Finally, Galactic tides may affect dark matter and stars differently, especially if stars are, as expected, strongly segregated relative to the dark halo. Thus a dwarf may today inhabit a relatively low-mass halo (say, below the threshold mentioned above) even though it actually formed in a massive one that has since seen much of its mass stripped away by tides (Kravtsov, Gnedin & Klypin 2004).

This paper is the first in a series that attempt to address these issues by interpreting available observational

³ We consider in this paper the “traditional” dwarfs brighter than $M_v \sim -8$ but recent discoveries based on the SDSS have uncovered the presence of many fainter dwarfs, extending the galaxy luminosity function to as faint as a few thousand L_\odot (e.g. Irwin et al. 2007 and references therein)

TABLE 1
OBSERVATIONAL PROPERTIES OF THE LOCAL GROUP DWARF SPHEROIDALS CONSIDERED IN THIS PAPER

Name	$\sigma_p(0)$ (km/s)	R_c (kpc)	R_t (kpc)	D (kpc)	l ($^\circ$)	b ($^\circ$)	l
Fornax	10.5 ± 2	0.400	2.078	138 ± 8	237.1	-65.7	-
Leo I	8.8 ± 1	0.169	0.645	250 ± 30	226.0	+49.1	-
Sculpt	6.6 ± 1	0.101	1.329	79 ± 4	287.5	-83.2	-
Leo II	6.7 ± 1	0.162	0.487	205 ± 12	220.2	+67.2	-
Sextans	6.6 ± 1	0.322	3.100	86 ± 4	243.5	+42.3	-
Carina	6.8 ± 2	0.177	0.581	101 ± 5	260.1	-22.2	-
UMi	9.3 ± 2	0.196	0.628	66 ± 3	105.0	+44.8	-
Draco	9.5 ± 2	0.158	0.498	82 ± 6	86.4	+34.7	-
And VII	—	0.450	4.300	763 ± 35	109.5	-9.9	-
And II	(9.3 ± 3)	0.362	2.650	652 ± 18	128.9	-29.2	-
And I	—	0.580	2.300	745 ± 24	121.7	-24.9	-
And VI	—	0.480	1.400	783 ± 25	106.0	-36.3	-
Cetus	(17 ± 2)	0.290	7.100	755 ± 23	101.5	-72.8	-
And III	—	0.290	1.500	749 ± 24	119.3	-26.2	-
And V	—	0.280	1.200	774 ± 28	126.2	-15.1	-
And IX	$(6.8-12)$	0.296	1.300	765 ± 24	123.2	-19.7	-

data on Local Group dwarfs in the cosmological context defined by the leading paradigm of structure formation; the cold dark matter theory. We start by considering the constraints on CDM halos placed by the structural and dynamical properties of the dwarfs, and use these results to try and interpret the origin of structural differences in the population of dwarfs that orbit M31 and the Milky Way, respectively. A future paper on the subject will analyze in detail the effects of Galactic tides, both in the survival of the stellar components, as well as on the observational signatures imprinted by stripping (Peñarrubia, Navarro & McConnachie in prep.).

The paper is organized as follows. Section 2 introduces the relevant observations and the modeling procedure, whereas §3 applies the models to the Milky Way dwarfs. We apply these results to M31 dwarfs in §4, and conclude with a brief summary in §5.

2. PRELIMINARIES

2.1. Summary of Observations

Table 1 lists the observational parameters of the Local Group dwarfs that we study here. We split the dwarfs into two groups, and list each in order of decreasing luminosity. The first set of objects are Milky Way (MW) dwarf spheroidals (dSphs), whereas the second set are all dSph type systems for which accurate core and tidal radii from King-model fitting are available. Most of the latter satellites orbit around M31, except for Cetus which is one of only two isolated dSphs in the Local Group.

Table 1 lists the Galactic coordinates of each dwarf (l and b), as well as its heliocentric distance, D . Distances are taken from McConnachie et al (2004, 2005) where available, otherwise from the compilation by Mateo (1998). Absolute magnitudes (M_v), core (R_c) and tidal (R_t) radii for the best-fitting King profiles to the surface brightness distribution are taken from Irwin & Hatzidimitriou (1995) for the MW satellites and from McConnachie & Irwin (2006) for Cetus and the M31 population, and are quoted after rescaling to the adopted distance. One exception is And IX, with core and tidal radii taken from Harbeck et al. (2005), distance from McConnachie et al. (2005), and the absolute magnitude from Zucker et al. (2004). The other is And II,

the one dSph in the Local Group whose surface brightness profile shows evidence for the presence of more than one dynamical component (McConnachie & Irwin 2006, McConnachie, Arimoto & Irwin 2007)) and where single King model fits are a poor description of the structure of the dwarf. In this case, we quote the And II core radius used by (Côté et al. 1999), since this is consistent with the traditional definition of core radius as the distance from the center where the surface brightness drops by a factor of two.

The central velocity dispersions ($\sigma_p(0)$) for the MW population in Table 1 are taken from the compilation by Mateo (1998) (his Table 7), although we note that since the publication of that review velocities for hundreds of stars in these dSphs have been measured with the aid of multi-object spectrographs. These data constrain the velocity dispersion profiles, $\sigma_p(R)$, in these systems, which are found to be approximately flat out to the nominal tidal radius (see, e.g., Fornax, Walker et al. 2006a, Battaglia et al. 2006; Leo I, Koch et al. 2006; Sculptor, Tolstoy et al. 2004, Westfall et al. 2006; Leo II, Sohn et al. 2006; Sextans, Walker et al. 2006b; Carina, Muñoz et al. 2006; Draco and Ursa Minor, Wilkinson et al. 2004, Muñoz et al. 2005). Note that the presence of several distinct components may affect the measured kinematics of a dwarf, depending on the spatial distribution of the tracers for which velocities are available (see, e.g., McConnachie, Peñarrubia & Navarro 2006, and references therein). We neglect here complications that arise from this issue, although we plan to address this in future work.

Kinematic data for the M31 dwarf population is scarce and, comparatively, of poorer quality. For example, Chapman et al (2005) find that the velocity dispersion of And IX is $\sim 6.8 \pm 3$ km/s, but note that adding a single (possible member) star to their sample raises this estimate to ~ 12 km/s. Similarly, the velocity dispersion for And II (Côté et al. 1999) is based on just seven stars and is thus subject to sizable uncertainty. The $\sigma_p(0)$ estimate for Cetus (Lewis et al 2006) is based on a larger sample of stars and it is likely more reliable. We present these data in Table 1 between parenthesis in order to emphasize that these data are not of the same quality as is available for the MW dSphs. We return to this issue in §4.

The past few years have seen a dramatic increase in the number of dwarf satellites discovered around M31 and the MW, in particular as a result of the completion of the Sloan Digital Sky Survey (Zucker et al. 2004, 2006a,b,c, Willman et al. 2005, Belokurov et al. 2006, 2007, Martin et al. 2006, Irwin et al. 2007). Many of these systems are morphologically not unlike the ones listed in Table 1, but they are typically much fainter and of much lower surface brightness. Their exact nature is unknown, but their irregular morphologies, occasional association with putative tidal streams, and the generally poorer available data, preclude for the time being their inclusion in the sample we consider here.

2.2. Modeling

Our dwarf galaxies models assume the presence of two components in dynamical equilibrium: (i) a stellar component approximated by a King (1966) model, and (ii) a dark matter halo, which we approximate using an NFW

profile (Navarro, Frenk & White 1996, 1997). We assume that the dark matter dominates the dynamics of the system, and that stars may be regarded as massless tracers of the potential.

2.2.1. Luminous component

The density profile of a King model may be written as (King 1962)

$$\rho_\star(r) = \frac{K}{x^2} \left[\frac{\cos^{-1}(x)}{x} - \sqrt{1-x^2} \right], \quad (1)$$

where

$$x \equiv \frac{1 + (r/r_k)^2}{1 + (r/r_t)^2}. \quad (2)$$

Here $\rho_\star(r > r_t) = 0$; r_k is an inner radial scale; r_t is the King “tidal” radius; and K is an arbitrary normalizing constant.

In the absence of rotation, the stellar kinematics is determined by the *total* gravitational potential, $\Phi(r)$, through Jeans’ equations. In particular, the radial velocity dispersion of stars, σ_r , is given by

$$\sigma_r^2 = \frac{1}{r^{2\beta} \rho_\star} \int_r^{r_t} r^{2\beta} \rho_\star \frac{d\Phi}{dr} dr, \quad (3)$$

(Binney & Tremaine 1987), where β is the velocity anisotropy. We shall assume hereafter that the stellar velocity distribution is isotropic ($\beta = 0$), which implies that the (observable) stellar line-of-sight velocity dispersion, $\sigma_p(R)$ is given by

$$\sigma_p^2(R) = \frac{2}{\Sigma(R)} \int_R^{r_t} \frac{\rho_\star \sigma_r^2 r}{\sqrt{r^2 - R^2}} dr, \quad (4)$$

where R is the projected radius and $\Sigma(R)$ is the projected stellar density,

$$\Sigma(R) = 2 \int_R^{r_t} \frac{r \rho_\star}{\sqrt{r^2 - R^2}} dr. \quad (5)$$

We follow traditional convention and define the (projected) core radius, R_c , by the condition $\Sigma(R_c) = \Sigma(0)/2$. The core radius, defined this way, depends on both of the King model parameters, r_k and r_t . For example, $R_c = 0.57 r_k$ for $r_t/r_k = 10$.

2.2.2. Dark matter component

We assume that dark matter halos may be approximated by NFW profiles (Navarro et al 1996, 1997). The density profile may be written as

$$\rho_{\text{NFW}} = \frac{M_{\text{vir}} (r/r_s)^{-1} (1+r/r_s)^{-2}}{4\pi r_s^3 [\ln(1+c) - c/(1+c)]}, \quad (6)$$

where M_{vir} is the mass within the virial radius, r_{vir} , r_s is the scale radius and c is the concentration ($c \equiv r_{\text{vir}}/r_s$). The virial radius is defined so that the mean overdensity relative to the critical density is Δ_{vir} ,

$$\frac{M_{\text{vir}}}{(4/3)\pi r_{\text{vir}}^3} = \Delta_{\text{vir}} \rho_{\text{crit}} = \Delta_{\text{vir}} \frac{3H(z)^2}{8\pi G}, \quad (7)$$

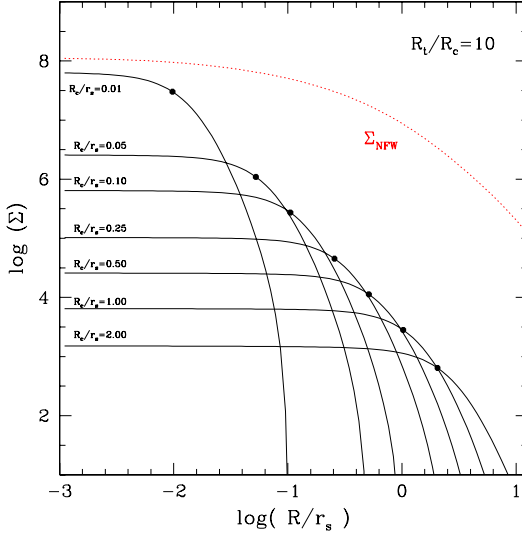


FIG. 1.— Stellar surface density profile of King models with the same “concentration”, $R_t/R_c = 10$, and various degrees of spatial segregation relative to the dark matter. The segregation is emeasured by the ratio R_c/r_s , where r_s is the scale radius of the NFW halo, shown by a dotted line in the figure and R_c is the stellar core radius denoted with a dot in each profile. All radii have been scaled to the scale radius of the NFW profile. Units of surface density are arbitrary, since stars are assumed to contribute negligibly to the potential of the system.

so that

$$r_{\text{vir}}(z) = \frac{75 h^{-1} \text{kpc}}{1+z} \left(\frac{M_{\text{vir}}}{10^{11} h^{-1} M_\odot} \frac{200}{\Omega_0 \Delta_{\text{vir}}(z)} \right)^{1/3}. \quad (8)$$

We follow Bryan & Norman (1998) and define the over-density by

$$\Delta_{\text{vir}}(z) = 18\pi^2 + 82 f(z) - 39 f(z)^2 \quad (9)$$

where

$$f(z) = \frac{\Omega_0(1+z)^3}{\Omega_0(1+z)^3 + \Omega_\Lambda} - 1. \quad (10)$$

We assume throughout the paper a Λ CDM Universe by fixing the cosmological parameters to $\Omega_0 = 0.3$, $\Omega_\Lambda = 0.7$, $h = 0.7$, $n = 1$, and $\sigma_8 = 0.9$, consistent with constraints from CMB measurements and galaxy clustering (see Spergel et al 2006 and references therein).

Finally, we note that an NFW profile is fully determined by two characteristic parameters, such as the virial mass and the concentration. However, because the virial definitions adopted above depend on redshift, it is sometimes preferable to characterize an NFW halo by the location of the circular velocity peak, $(r_{\text{max}}, V_{\text{max}})$, where

$$V_{\text{max}} \equiv V_{\text{NFW}}(r_{\text{max}}) \simeq \left[\frac{GM_{\text{vir}}}{2r_s} \frac{\ln(3) - 2/3}{\ln(1+c) - c/(1+c)} \right]^{1/2}, \quad (11)$$

and $r_{\text{max}} \simeq 2r_s$.

Although the two characterizations are equivalent, we shall adopt the latter in this paper, since it is independent of redshift and its parameters are more easily compared with observation.

3. KING MODELS EMBEDDED IN NFW HALOS

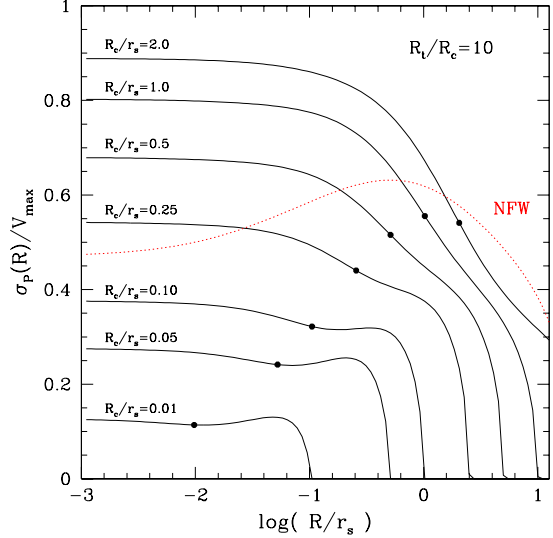


FIG. 2.— Stellar projected velocity dispersion profiles normalized to the halo maximum circular velocity for different values of R_c/r_s . The dotted line represents the projected velocity dispersion profile of the NFW halo. The solid circles indicate the core radius of the King model. Note that both the central velocity dispersion of the stars, as well as the shape of the velocity dispersion profile, depend on the degree of spatial segregation between stars and dark matter (quantified here by the ratio R_c/r_s).

3.1. Spatial segregation and velocity dispersion

Stars that follow a King model and inhabit an NFW halo have their kinematics dictated principally by the spatial segregation of stars relative to dark matter, which may be quantified by the ratio of King “core” radius to NFW scale radius, R_c/r_s . The more concentrated the stars are relative to the dark matter, the smaller the velocity of the stars will be relative to the characteristic circular velocity of the dark matter dominated potential.

Fig. 1 shows the projected density profile of King models as a function of R_c/r_s , and compares them to an NFW profile. The radial units are scaled to the NFW scale radius, r_s , and the vertical units are arbitrary in this plot. The corresponding velocity dispersion profiles are shown in Fig. 2. Velocities have been scaled to the peak circular velocity of the NFW halo, V_{max} , and show clearly the anticipated behaviour: the deeper the stars are embedded within the halo, the smaller the stellar velocities. For example, if $R_c \sim 0.1r_s$, the stellar central velocity dispersion, $\sigma_p(0)$, is only about 40% of V_{max} , but this value rises to 80% for $R_c \sim r_s$. There is also a weak dependence on the tidal radius, but this is minor, as discussed below.

This implies that a “family” of NFW halos is consistent with a King model of given R_c and $\sigma_p(0)$ (see Strigari et al 2006 for a similar argument applied to the Fornax dSph). The more embedded we assume the King model to be within the NFW halo, the more massive (i.e., higher V_{max}) the halo must be in order to explain a given $\sigma_p(0)$. This “King-NFW degeneracy” is illustrated in Figure 3, where the thick lines show the correspondence between $V_{\text{max}}/\sigma_p(0)$ and r_{max}/R_c . The three thick lines (almost indistinguishable from one another in this panel) correspond to three different values of the tidal-to-core radius ratio chosen for the King model, and confirm the result anticipated above regarding the weak dependence on R_t

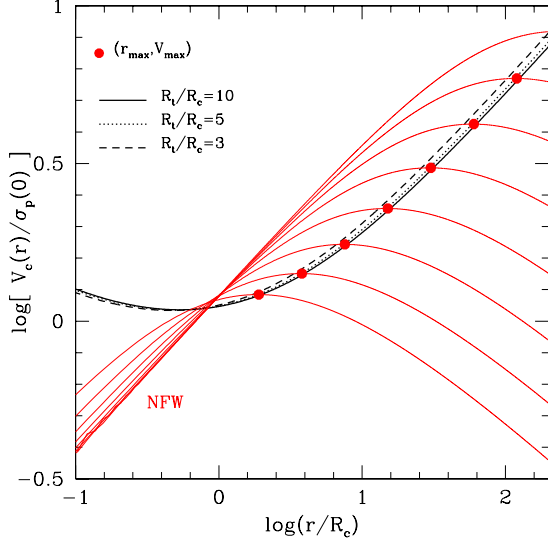


FIG. 3.— The King-NFW degeneracy. The thick lines show the halo peak circular velocity, V_{\max} , in units of the central velocity dispersion, and the radius of the peak, r_{\max} , in units of the King model core radius. Solid, dotted and dashed lines denote different King-model concentrations (R_t/R_c). Any NFW halo whose circular velocity peaks along this curve is consistent with the King model structure and kinematics. A few of these NFW models are shown for illustration by the thin curves. Note that all these NFW models cross each other at approximately $R \simeq R_c$ and $V_c \simeq 1.2 \sigma_p(0)$. This implies that, given our assumptions, the mass within the core radius of the stellar component is robustly constrained to be $M(R_c) \sim 1.44 R_c \sigma_p^2(0)$.

of these results.

Any NFW halo whose circular velocity peaks somewhere along the thick curve in Figure 3 is, therefore, consistent with a King model of given $\sigma_p(0)$ and R_c . A few examples of NFW halos belonging to this “family” are shown by the thin lines in Figure 3. Note that essentially all the circular velocity profiles of these halos, despite having very different masses and concentrations, cross each other at $r \approx R_c$. This implies that the total enclosed mass within the core radius of a King model is robustly determined given our assumptions: in particular, we find $V_c(R_c) \simeq 1.2 \sigma_p(0)$ and $M(R_c) \simeq 1.44 R_c \sigma_p(0)^2/G$. Physically, this means that, although the *total* mass and radial extent of the halo are not well pinned down, the mass within the luminous region sampled by the tracers is.

A further constraint may be gleaned from Fig. 2, which shows that the *shape* of the stellar velocity dispersion profile also depends on the degree of segregation between stars and dark matter. For $R_c \lesssim 0.1 r_s$ ($= 0.05 r_{\max}$) the velocity profile remains approximately flat well outside the core radius, and declines abruptly only at the “tidal” radius. On the other hand, less segregated King models show a steep velocity decline noticeable near the core radius: for example, for $R_c \sim r_s$ the velocity dispersion declines by roughly 70% at the core radius from the central value. The velocity dispersion profiles of all dwarfs for which such data are available show little sign of declining outside R_c (see references in § 2.1). In the context of our modeling, this suggests that the stellar component is deeply embedded within its parent CDM halo (i.e., $R_c \lesssim r_{\max}$), an issue to which we return below.

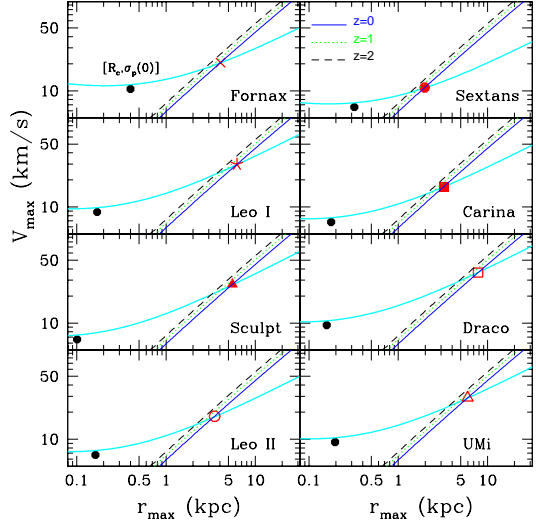


FIG. 4.— Each panel shows, for the 8 Milky Way dwarfs in our sample, the King-NFW degeneracy (curved line), as well as the predictions for Λ CDM cosmogony (set of straight lines). Only NFW halos at the intersection of both sets of curves (marked by a red symbol) are consistent with both cosmological constraints and the structure and kinematics of the dwarfs. The three sets of cosmological curves correspond to NFW halos identified at various redshifts; we adopt the $z = 0$ models here, but note that our conclusions are unlikely to be severely affected by this choice.

3.2. Application to Milky Way dwarfs

One way of breaking the degeneracy illustrated in Figure 3 is to appeal to the results of cosmological N-body simulations. These show that there is a strong correlation between the mass and concentration of a CDM halo or, equivalently, between r_{\max} and V_{\max} . This correlation is now well established, and a number of authors provide simple formulae to compute it once the cosmological parameters are specified (NFW, Eke, Navarro & Steinmetz 2001, Bullock et al 2001).

The relation between V_{\max} and r_{\max} implies that, of all NFW halos in the “family” of models allowed for a given dwarf by the degeneracy illustrated in Figure 3, a single one will be consistent with the parameters expected in a given cosmogony. This is shown in Figure 4, where the curved lines show, in different panels and for each of the eight MW dSph, the King-NFW “degeneracy” relation. The straight lines in each panel delineate the V_{\max} - r_{\max} relation consistent with the Λ CDM cosmogony. The set of three straight lines correspond to NFW halos identified at $z = 0, 1$, and 2 , respectively. We shall hereafter ignore the relatively small difference between these curves and refer, for simplicity, all of our results to $z = 0$.

In each panel a solid dot indicates, for reference, the core radius and the central velocity dispersion of each galaxy, as listed in Table 1. All of these points lie well to the left of the cosmological relations, confirming our earlier suggestion that the luminous components are significantly segregated within their dark halos (i.e., they are substantially smaller for given characteristic velocity).

The intersection between the King-NFW degeneracy and the cosmological relation is marked by red symbols for each dwarf. This indicates the parameters of the NFW halo model that is consistent with the Λ CDM cos-

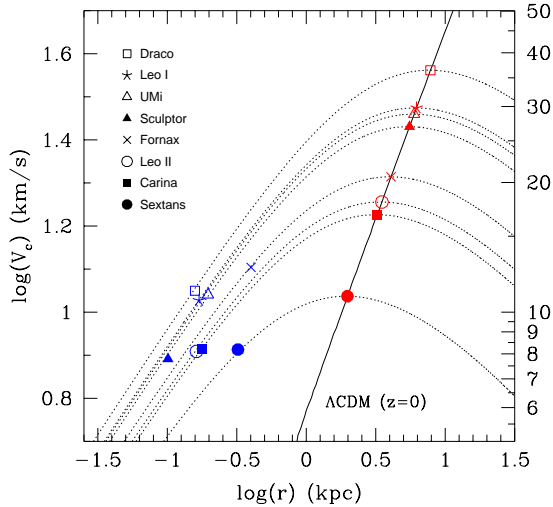


FIG. 5.— Circular velocity profiles of NFW halo models consistent with the observed structure and kinematics of the stars and with the Λ CDM cosmological constraints. Blue symbols (on the left) denote the circular velocity at the core radius of each dwarf, where it is best constrained. Labels rank, from top to bottom, all dwarfs in decreasing order of halo mass.

mogony and, at the same time, matches the kinematics and structure of each dwarf galaxy. The circular velocity profiles of the eight NFW halos satisfying these criteria are shown in Fig. 5, and labelled from top to bottom in order of decreasing halo mass.

This ranking shows interesting peculiarities. For example, it shows that the peak circular velocities of dwarf halos vary from ~ 17 to ~ 35 km/s, corresponding to a spread of about 8 in mass, much narrower than the factor of ~ 70 spanned by dSph luminosities. Note as well that, as anticipated in §1, halo mass is not monotonically related to luminosity. Intriguingly, Draco, one of the faintest dwarfs in our sample, is assigned the most massive halo, whereas Fornax, despite being 70 times brighter, is assigned a halo 5 times less massive.

The lack of correlation between luminosity and halo mass is shown explicitly in Figure 6, where we plot, as a function of total visual magnitude, the virial mass of the halo (red symbols at the top), as well as the mass within the core radius of each dwarf (blue symbols at bottom). Symbols are the same as those used in Fig. 5 to denote different galaxies.

Note that the total mass within the core radius—a fairly robust measure according to our discussion of Fig. 3—is approximately independent of luminosity⁴. This implies that the *average density* of dark matter will be higher in physically smaller systems such as Draco than in more extended dwarfs such as Fornax. Why does this matter? Because more massive halos are denser than less massive ones *at all radii* in the CDM cosmogony. Indeed, note that the circular velocity profiles of the NFW halos shown in Figure 5 do not cross, which means that measuring the halo circular velocity (or mass) at *any* radius leads to a well-defined estimate of the *total* mass of the halo. Because Draco, despite being faint, has a cir-

⁴ This is not a new result, and is consistent with Mateo's (1998) conclusion that simple dynamical mass estimates of dwarf galaxies are independent of luminosity.

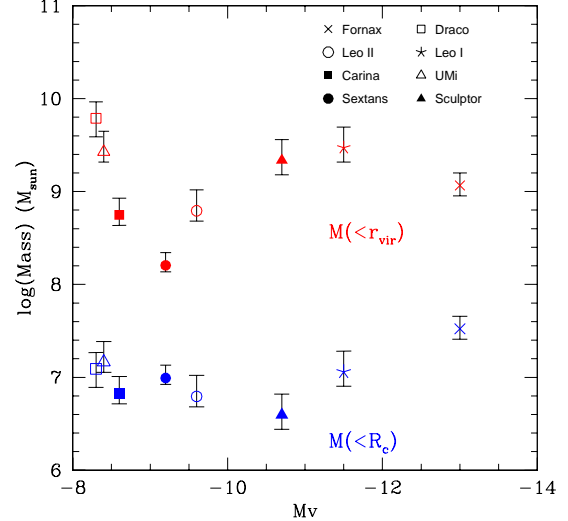


FIG. 6.— Virial masses inferred from the NFW halo models shown in Fig. 5 for each of the 8 MW dwarfs. Also shown is the mass enclosed within R_c for these systems. Error bars show the dependence of M_{vir} on the redshift adopted for the cosmological $V_{\text{max}} = V_{\text{max}}(r_{\text{max}}, z)$ relation. Top of the error bar corresponds to $z = 0$, the bottom to $z = 2$. Note that all dwarfs, irrespective of luminosity, have approximately the same mass within their core radii.

cular velocity comparable to Fornax's at a much smaller radius, it requires a denser, and therefore more massive, halo to satisfy the observational constraints.

Of the eight dwarfs, the lowest halo mass corresponds to Sextans, whose relatively large radius and small velocity dispersion is inconsistent with a very massive CDM halo. However, we note that this system is quite irregular in morphology, and it is possible that tides may have affected significantly its structure.

3.3. Effects of tidal stripping

The results obtained in the previous section assume that the structure of dark matter halos is well approximated by an NFW profile. Although this assumption may be appropriate for isolated halos, it is unlikely to hold in detail for “substructure” halos of dSphs orbiting within the main halo of the Milky Way. Recently, Stoehr et al (2002), Hayashi et al (2003) and Kazantzidis et al (2004) have examined the modifications undergone by an NFW halo as it is tidally stripped inside a more massive system. Stripping affects principally the outer regions of the halo, and therefore deeply embedded stellar structures may survive unscathed the removal of large fractions of their halos.

This is illustrated in Figure 7, which shows the circular velocity profile of an NFW halo, after being tidally stripped of 50%, 75%, and 90% of its mass, respectively. The profiles are taken from N-body simulations of NFW halos orbiting within the potential of a much larger system, as in Hayashi et al (2003). Figure 7 indicates that NFW halos must lose at least 90% of their original mass before regions within $r \lesssim 0.1 r_{\text{max}}$ are significantly affected. Interestingly, this is precisely the region that our analysis suggests is populated by the stars of MW dwarfs. According to Fig. 5 the average R_c/r_{max} for all MW dwarfs is 0.054 and they all have, with the possible exception of Sextans, $R_c \lesssim 0.1 r_{\text{max}}$. Dwarfs may

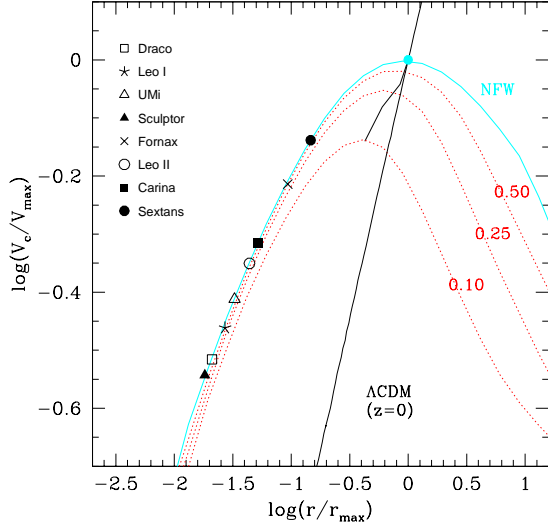


FIG. 7.— NFW halo circular velocity, normalized to the location of the peak. The core radius of each of the MW dwarf galaxies is shown. Note that, except for Sextans, in all cases the core radius lies within $0.1 r_{\max}$. Dotted lines show the changes imposed by tidal stripping, as the original NFW halo loses 50%, 75%, and 90% of its mass. Note that most dwarfs are sufficiently embedded within their halos that they would only be affected if the halo lost more than $\sim 90\%$ of their original mass.

therefore lose most of their halo mass before the stellar component shows evidence of tidal stirring. The deep segregation between stars and dark matter also predicts that $\sigma_p(R)$ profiles should not decline in the outskirts of a dwarf, consistent with the few dSphs where such data are available (see § 3.1).

The lack of overwhelming evidence for ongoing stripping of stars from most dSphs (except for the Sagittarius dwarf; although see Majewski et al. 2005, Muñoz et al. 2006 for a different viewpoint) may thus be taken to imply that dwarf halos have retained at least 10% of their original mass. This is important, because even for such sizeable loss, the peak circular velocity of the halo is barely affected.

The thin line in Figure 7 tracks the position of the circular velocity peak of an NFW halo as it is tidally stripped, and shows that halos that have lost 75% of their mass to stripping see only a 10% decrease in V_{\max} . Even after losing 90% of its mass, a halo sees its V_{\max} reduced by only $\sim 30\%$ ⁵. We conclude, therefore, that, unless dSphs have suffered catastrophic tidal losses, our estimates of the peak circular velocities for the MW dSphs (Fig. 5) should be relatively robust. Strictly speaking, however, the (r_{\max}, V_{\max}) parameters derived above for each MW dwarf should be interpreted as lower limits to the original NFW halo parameters.

3.4. Application to the “satellite crisis”

The analysis of the preceding subsections suggests that the 8 MW dwarfs chosen for our analysis inhabit halos with peak circular velocities in the range 17–35 km/s, a factor of ~ 3 higher than their central (stellar) velocity dispersions. As discussed by Stoehr et al (2002),

⁵ The location of the peak, r_{\max} , on the other hand, is more significantly affected, and shifts inwards by almost a factor of ~ 3 after a halo loses 90% of its mass.

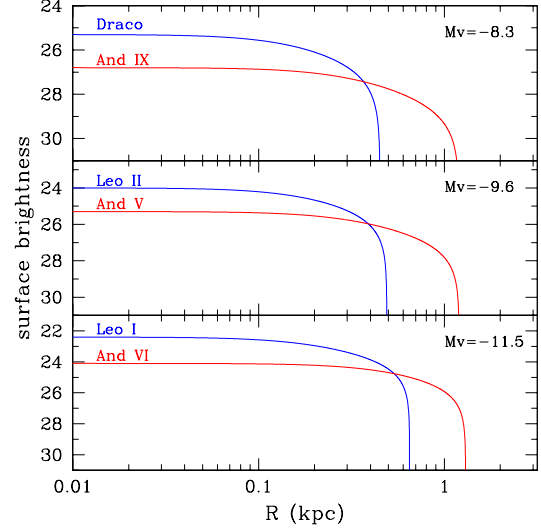


FIG. 8.— Comparison of the surface density profile of pairs of dwarf galaxies of similar luminosity, one orbiting around M31 and the other around the Milky Way. On average M31 dwarfs are larger and have lower surface brightness than their MW counterparts.

Hayashi et al (2003) and Kazantzidis et al (2004), this correction is enough to alleviate substantially the “satellite crisis” highlighted by Klypin et al (1999) and Moore et al (1999).

In rough terms, N-body simulations show that there are typically about 20–30 substructure halos with peak circular velocities exceeding 10% of the main halo’s virial velocity (see, e.g., Diemand, Kuhlen & Madau 2006 for recent results, and references therein). According to our analysis, there are about a dozen dwarfs with $V_{\max} \gtrsim 17$ km/s (adding to our sample brighter satellites such as the Magellanic Clouds). This velocity corresponds to between 8 and 10% of the MW virial velocity, assuming, as seems likely, that the latter is in the range 170–220 km/s. This factor of ~ 2 discrepancy between the number of massive dark matter substructures and luminous satellites does not appear extravagant given the uncertainties. Furthermore, the discrepancy may disappear altogether if (as the scenario outlined in § 1 would suggest) the ultra-faint MW dwarfs identified in SDSS data turn out to inhabit halos of masses comparable to those of the 8 dSphs we consider here. Since these newly discovered dwarfs have, on average, similar physical sizes to the dSphs in Table 1, we expect that their velocity dispersions will also be comparable and in the range ~ 6 –10 km/s, a prediction of this CDM-motivated modeling that should be testable in the near future.

Indeed, further progress on this subject seems imminent, as observational campaigns secure velocity dispersions for many of the newly discovered dwarfs and extend available data to allow for velocity dispersion profiles to be measured for more systems. One also expects that numerical simulations will improve to the point that a reliable direct estimate of the number of substructure halos satisfying the $M(R_c)$ constraints shown in Fig. 6 will be possible, obviating the need to extrapolate results out to the peak of the halo circular velocity curve. The latter goal requires simulations able to resolve convincingly the inner ~ 100 pc of substructure halos, an order of magnitude improvement over simulations published so

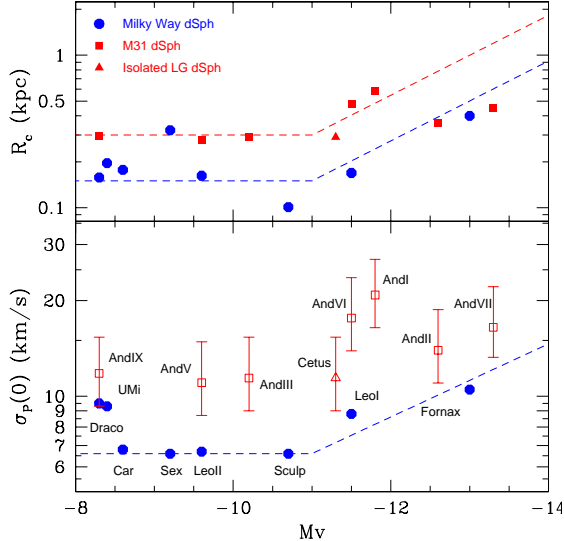


FIG. 9.— *Upper panel*: Core radii of Milky Way (filled circles) and M31 (filled squares) dwarf galaxies as a function of their absolute magnitude. The dashed lines are intended to guide the eye and to highlight the difference in size between the M31 and MW dwarf populations. *Bottom panel*: Measured (filled symbols) and *predicted* (open symbols) central velocity dispersions if the Milky Way and M31 dSph's are embedded in similar dark matter halos. See text for details.

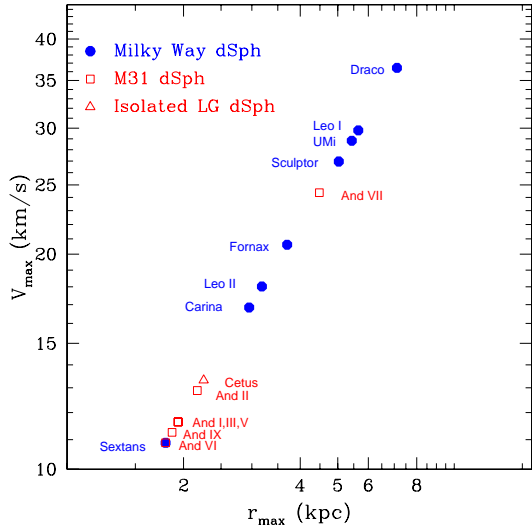


FIG. 10.— NFW halo parameters (r_{\max} , V_{\max}) for the Milky Way (filled circles) and M31 (open squares) dwarf galaxies expected if the velocity dispersion of M31 dwarfs are found to be similar to those of their MW counterparts. Note that these assumptions lead to dark matter subhalos in M31 that are substantially smaller than those in the Milky Way, a result which is disfavored by the present analysis. See text for details.

far. This is a numerical challenge that will likely be met soon but that will nevertheless require the investment of massive computational resources.

4. MILKY WAY VS. M31 DWARFS

Photometric studies of the dwarf galaxies in the Local Group (Irwin & Hatzidimitriou 1995, McConnachie & Irwin 2006) have shown that, at fixed luminosity, M31 dwarfs are considerably more extended than their Milky Way counterparts (see Table 1). We illustrate this in

Fig. 8, where King model fits to the surface brightness profiles of three pairs of dwarfs of similar luminosity are shown. Each pair consists of one M31 satellite and one MW satellite, respectively. Clearly, the M31 dwarfs are systematically different: they are about 1.5 mag fainter in central surface brightness and about a factor of two larger in radial extent compared with MW dwarfs (see top panel of Fig. 9).

The origin of this difference is unclear, but it offers nonetheless a way of assessing the general validity of the modeling proposed in the previous sections. Indeed, under the plausible assumption that the dark matter halos of dwarfs in M31 and in the Milky Way are not systematically dissimilar, the arguments of § 3.1 imply that the difference in size of M31 dwarfs should be reflected in their kinematics through significantly higher velocity dispersions. Note that this prediction depends explicitly on the presence of dark matter halos whose mass and extent are largely independent from the stars', as implicitly assumed in our modeling so far. Other (also plausible?) assumptions, such as mass-traces-light, would lead to the *opposite* trend, and would predict systematically *lower* velocity dispersions.

In order to estimate quantitatively the velocity dispersion of M31 dwarfs we need to know how spatially segregated the stars are from the dark matter in these systems. Once this is fixed by, for example, assuming a value for the ratio R_c/r_{\max} , we can compute r_{\max} for each dwarf and, from that, infer V_{\max} assuming the cosmological relation between these parameters. Since the ratio R_c/r_{\max} also fixes $V_{\max}/\sigma_p(0)$ according to the King-NFW degeneracy shown in Fig. 3, an estimate can then be made of the central velocity dispersion, $\sigma_p(0)$, for each M31 dwarf.

We have followed this procedure, assuming $R_c/r_{\max} = 0.05$, consistent with the average segregation measure derived for MW dwarfs (see Fig. 7), as well as with the flat $\sigma_p(R)$ constraint mentioned in § 3.1. This leads to the estimates of the velocity dispersions of M31 dwarfs plotted in the bottom panel of Fig. 9 (open symbols). Error bars show the variation induced in the estimate by allowing R_c/r_{\max} to vary between 0.025 and 0.1. Clearly, the velocity dispersion of M31 dSphs is significantly larger (by about a factor of ~ 2) than that of their MW counterparts, as shown by the shift between solid circles and open symbols in Fig. 9.

We emphasize that these “predictions” for the velocity dispersions of M31 dwarfs should be taken with caution: indeed, the open symbols in Fig. 9 are best interpreted as *indicative* of the relative shift in the velocity dispersion of the *population* of M31 dwarfs rather than as separate individual predictions.

So far, the few available observations are consistent with the predicted trend. Of the three dwarfs outside the MW for which velocity dispersions have been published (see, Table 1), the most reliable is Cetus and, at 17 km/s, has the highest σ_p in the sample, consistent with the predicted trend. Likewise, the higher of the two estimates derived by Chapman et al (2005, 12 km/s) for And IX is also consistent with this trend, although the very few stars in this galaxy (as well as in And II) with measured velocities suggest that it would be premature to draw firm conclusions until the data improves substantially.

It is clear, however, that should future observations fail to confirm the predicted trend, one or many of our assumptions would need to be revised. As an illustrative example, we consider how our interpretation would change if the velocity dispersion of M31 dwarfs were to show no systematic departure from that of their MW counterparts (i.e., if the open symbols were found to align with the dashed line in the bottom panel of Fig. 9). In this case, one would be forced to conclude that M31 and MW dwarfs of similar luminosity inhabit systematically different halos. In particular, M31 dwarf halo hosts would need to be significantly less massive (i.e., lower V_{\max} and smaller r_{\max}) in order to accommodate their larger physical size but similar kinematics.

This is shown in Fig. 10, and imply that essentially all M31 dwarfs considered here would have $V_{\max} \lesssim 15$ km/s (with the possible exception of And VII). Since, in all likelihood, M31 inhabits a halo at least as massive as the Milky Way's, it should have at least as many massive substructures as our own Galaxy, and one would need to explain why those substructures have not “lit up” in M31 as they have in the Milky Way. We consider this a compelling argument against this interpretation and in support of higher velocity dispersions for M31 dwarfs as the most natural prediction of CDM-motivated models of the Local Group dSphs.

One last possibility should be mentioned; namely, that the structural differences between M31 and MW dwarfs reflect differences in the dynamical evolution driven by tides in M31 and the Galaxy. Although we have argued in §3.3 that this is unlikely, a definitive assessment requires high-resolution, self-consistent N-body simulations of how tides affect multiple-component models of dSph galaxies. We plan to address this issue in the near future (Peñarrubia, Navarro & McConnachie, in preparation).

5. SUMMARY

We have considered in this paper the observational constraints placed on the mass and spatial extent of cold dark matter halos surrounding Local Group dwarf spheroidal galaxies. Assuming that the luminous component may be approximated by King models and that dark halos follow the NFW mass profile, we conclude that estimates of the halo mass of a dSph depend principally on the degree of spatial segregation between stars and dark matter: the more embedded the stars within the dark halo the more massive the halo must be in order to explain the observed stellar kinematics. This degeneracy may be broken by appealing to the results of cosmological N-body simulations—which indicate a strong correlation between mass and size of cold dark matter halos. The

procedure results in reasonably robust estimates of the *original* dark halo mass of a dSph and of its peak circular velocity.

Our analysis indicates that the mass within the luminous radius of the dwarf is well constrained by the velocity dispersion of the stars, and that it is approximately independent of the luminosity of the system. Within the context of cosmologically motivated CDM halos, this implies that dSphs are surrounded by halos with peak circular velocities a factor of ~ 3 times larger than their stellar velocity dispersion. These results are consistent with previous work, and substantially alleviate the “missing satellites” problem, particularly if most of the newly discovered ultra-faint satellites are confirmed to be bona-fide dwarf galaxies akin to the more luminous, classical systems analyzed here.

We also find that stars in dSphs are deeply embedded within their dark matter halos, with core radii typically of order 5% the radius where the original halo circular velocity peaks. This renders dSphs fairly resilient to tidal disruption; a halo would need to lose more than 90% of its mass before stars begin to be affected. Even in this case, however, the peak circular velocity of a halo would only drop by $\sim 20\%$, suggesting that our V_{\max} estimates are robust even if halos have been heavily (but perhaps not catastrophically) affected by tidal stripping.

Applied to the dSph population of M31, this analysis suggests that the systematic difference in size between M31 dwarfs and their MW counterparts should be reflected in their kinematics. Under the plausible assumption that substructure halos in M31 are similar to those of the Milky Way, we conclude that, as a population, the velocity dispersion of M31 dwarfs should be $\sim 50\text{--}100\%$ higher than that of dwarfs in our own Galaxy.

This prediction is likely to be validated (or challenged) soon by the results of the many ongoing observational projects devoted to obtaining accurate spectra and radial velocities for stars in these galaxies. Whether Local Group dwarfs conform with the expectations of the prevailing CDM paradigm or throw it a further gauntlet we should know in the near future.

This work has been supported by various grants from the Natural Sciences and Engineering Research Council of Canada (NSERC). JP thanks Scott Chapman for all his help. JFN acknowledges useful discussions with Simon White and thanks Carlos Frenk and the Institute of Computational Cosmology of the University of Durham for their hospitality during the time that this work was carried out.

REFERENCES

Aaronson, M. 1983, ApJ, 266, L11
 Aaronson, M., & Olszewski, E. W. 1987, AJ, 94, 657
 Armandroff, T. E., Olszewski, E. W., & Pryor, C. 1995, AJ, 110, 2131
 Battaglia, G., Tolstoy, E., Helmi, A., Irwin, M. J., Letarte, B., Jablonka, P., Hill, V., Venn, K. A., Shetrone, M. D., Arimoto, N., Primas, F., Kaufer, A., Francois, P., Szeifert, T., Abel, T., & Sadakane, K. 2006, astro-ph/0608370
 Belokurov, V., et al. 2006, ApJ, 647, L111
 Belokurov, V., et al. 2007, ApJ, 654, 897
 Benson, A. J., Lacey, C. G., Baugh, C. M., Cole, S., & Frenk, C. S. 2002, MNRAS, 333, 156
 Binney J., Tremaine S., 1987, Galactic Dynamics. Princeton University Press, Princeton, New Jersey
 Bryan G., Norman M., 1998, ApJ, 495, 80
 Bullock J., Kravtsov A., Weinberg D., 2000, ApJ, 539, 517
 Bullock, J. S., Kolatt, T. S., Sigad, Y., Somerville, R. S., Kravtsov, A. V., Klypin, A. A., Primack, J. R., & Dekel, A. 2001, MNRAS, 321, 559
 Chapman, S. C., Ibata, R., Lewis, G. F., Ferguson, A. M. N., Irwin, M., McConnachie, A., & Tanvir, N. 2005, ApJ, 632, L87

Côté, P., Mateo, M., Olszewski, E. W., & Cook, K. H. 1999, *ApJ*, 526, 147

Diemand, J., Kuhlen, M., & Madau, P. 2006, ArXiv Astrophysics e-prints, arXiv:astro-ph/0611370

Efstathiou, G. 1992, *MNRAS*, 256, 43P

Eke, V. R., Navarro, J. F., & Steinmetz, M. 2001, *ApJ*, 554, 114

Harbeck, D., Gallagher, J. S., Grebel, E. K., Koch, A., & Zucker, D. B. 2005, *ApJ*, 623, 159

Hayashi, E., Navarro, J. F., Taylor, J. E., Stadel, J., & Quinn, T. 2003, *ApJ*, 584, 541

Irwin M., Hatzidimitriou D., 1995, *MNRAS*, 277, 1354

Irwin, M. J., et al. 2007, ArXiv Astrophysics e-prints, arXiv:astro-ph/0701154

Kauffmann, G., White, S. D. M., & Guiderdoni, B. 1993, *MNRAS*, 264, 201

Kazantzidis, S., Mayer, L., Mastropietro, C., Diemand, J., Stadel, J., & Moore, B. 2004, *ApJ*, 608, 663

King, I. 1962, *AJ*, 67, 471

King, I. R. 1966, *AJ*, 71, 64

Kleyna, J. T., Wilkinson, M. I., Evans, N. W., & Gilmore, G. 2004, *MNRAS*, 354, L66

Kleyna, J. T., Wilkinson, M. I., Evans, N. W., & Gilmore, G. 2005, *ApJ*, 630, L141

Klypin, A., Kravtsov, A. V., Valenzuela, O., & Prada, F. 1999, *ApJ*, 522, 82

Koch, A., Wilkinson, M. I., Kleyna, J. T., Gilmore, G. F., Grebel, E. K., Mackey, A. D., Evans, N. W., & Wyse, R. F. G. 2006, ArXiv Astrophysics e-prints, arXiv:astro-ph/0611372

Kravtsov, A. V., Gnedin, O. Y., & Klypin, A. A. 2004, *ApJ*, 609, 482

Kroupa, P. 1997, *New Astronomy*, 2, 139

Lewis, G. F., Ibata, R. A., Chapman, S. C., McConnachie, A., Irwin, M. J., Tolstoy, E., & Tanvir, N. R. 2006, ArXiv Astrophysics e-prints, arXiv:astro-ph/0612293

Majewski, S. R., et al. 2005, *AJ*, 130, 2677

Martin, N. F., Ibata, R. A., Irwin, M. J., Chapman, S., Lewis, G. F., Ferguson, A. M. N., Tanvir, N., & McConnachie, A. W. 2006, *MNRAS*, 371, 1983

Martínez-Delgado, D., Alonso-García, J., Aparicio, A., & Gómez-Flechos, M. A. 2001, *ApJ*, 549, L63

Mashchenko, S., Sills, A., & Couchman, H. M. 2006, *ApJ*, 640, 252

Mateo M.L., 1998, *ARA&A*, 36, 435

McConnachie, A. W., Irwin, M. J., Ferguson, A. M. N., Ibata, R. A., Lewis, G. F., & Tanvir, N. 2004, *MNRAS*, 350, 243

McConnachie, A. W., Irwin, M. J., Ferguson, A. M. N., Ibata, R. A., Lewis, G. F., & Tanvir, N. 2005, *MNRAS*, 356, 979

McConnachie A. W., Irwin M.J., 2006, *MNRAS*, 365, 1263

McConnachie A. W., Peñarrubia J., Navarro J.F., 2006, *ApJL* submitted, astro-ph/0608687

McConnachie A. W., Arimoto, N., Irwin, M.J., 2007, *ApJL* submitted

Moore, B., Ghigna, S., Governato, F., Lake, G., Quinn, T., Stadel, J., & Tozzi, P. 1999, *ApJ*, 524, L19

Muñoz, R. R., et al. 2005, *ApJ*, 631, L137

Muñoz, R. R., et al. 2006, *ApJ*, 649, 201

Navarro, J. F., Frenk, C. S., & White, S. D. M. 1996, *ApJ*, 462, 563

Navarro J., Frenk C.S., White S.D.M., 1997, *ApJ*, 490, 493 (NFW)

Palma, C., Majewski, S. R., Siegel, M. H., Patterson, R. J., Ostheimer, J. C., & Link, R. 2003, *AJ*, 125, 1352

Peñarrubia, J., & Benson, A. J. 2005, *MNRAS*, 364, 977

Peñarrubia, J., Kroupa, P., & Boily, C. M. 2002, *MNRAS*, 333, 779

Sohn et al. 2006, astro-ph/0608151, submitted to *ApJ*

Somerville, R. S. 2002, *ApJ*, 572, L23

Spergel, D. N., et al. 2006, ArXiv Astrophysics e-prints, arXiv:astro-ph/0603449

Stoehr, F., White, S. D. M., Tormen, G., & Springel, V. 2002, *MNRAS*, 335, L84

Strigari L., Bullock J., Kaplinghat M., Kravtsov A., Gnedin O., Abazajian K., Klypin A., astro-ph/0603775, submitted to *ApJ*

Tolstoy, E. et al. 2004, *ApJ*, 617, L119

Walker, M. G., Mateo, M., Olszewski, E. W., Bernstein, R., Wang, X., & Woodroffe, M. 2006a, *AJ*, 131, 2114

Walker, M. G., Mateo, M., Olszewski, E. W., Pal, J. K., Sen, B., & Woodroffe, M. 2006b, *ApJ*, 642, L41

Wang X., Woodroffe M., Walker M.G., Mateo M., Olszewski E., 2005, *ApJ*, 626, 145

Westfall, K. B., Majewski, S. R., Ostheimer, J. C., Frinchaboy, P. M., Kunkel, W. E., Patterson, R. J., & Link, R. 2006, *AJ*, 131, 375

White, S. D. M., & Rees, M. J. 1978, *MNRAS*, 183, 341

Wilkinson, M. I., Kleyna, J., Evans, N. W., & Gilmore, G. 2002, *MNRAS*, 330, 778

Wilkinson, M. I., Kleyna, J., Evans, N. W., & Gilmore, G. Irwin M.J., Grebel E.K., 2004, *ApJ*, 611, L21

Willman, B., et al. 2005, *ApJ*, 626, L85

Zentner, A. R., & Bullock, J. S. 2003, *ApJ*, 598, 49

Zucker, D. B., et al. 2004, *ApJ*, 612, L121

Zucker, D. B., et al. 2006, ArXiv Astrophysics e-prints, arXiv:astro-ph/0601599

Zucker, D. B., et al. 2006, *ApJ*, 643, L103

Zucker, D. B., et al. 2006, *ApJ*, 650, L41